Molecular Mechanism of PP2A/B55α Phosphatase Inhibition by IER5

Ruili Cao[1#], Daniel TD Jones[1#], Li Pan[2#], Annie Yang[1], Shumei Wang[2], Sathish K. R. Padi[3]

Shaun Rawson[1], Jon C Aster[2*], and Stephen C Blacklow[1,4*]

[1]Department of Biological Chemistry and Molecular Pharmacology, Blavatnik Institute, Harvard Medical School, Boston, MA, USA

[2]Department of Pathology, Brigham and Women's Hospital, Boston, MA, USA

[3]Department of Molecular Biology and Biophysics, University of Connecticut Health Center, Farmington, CT, USA

[4]Department of Cancer Biology, Dana Farber Cancer Institute, Boston, MA, USA

[#]Equal contributors

*Correspondence: stephen_blacklow@hms.harvard.edu; jaster@bwh.harvard.edu

ABSTRACT (150 words)

PP2A serine/threonine phosphatases are heterotrimeric complexes that execute many essential physiologic functions. These activities are modulated by additional regulatory proteins, such as ARPP19, FAM122A, and IER5. Here, we report the cryoelectron microscopy structure of a complex of PP2A/B55α with the N-terminal structured region of IER5 (IER5-N50), which occludes a surface on B55α used for substrate recruitment, and show that IER5-N50 inhibits PP2A/B55α catalyzed dephosphorylation of pTau in biochemical assays. Mutations of full-length IER5 that disrupt its PP2A/B55α interface interfere with co-immunoprecipitation of PP2A/B55α. These mutations and deletions that remove the nuclear localization sequence of IER5 suppress cellular events such as *KRT1* expression that depend on association of IER5 with PP2A/B55α. Querying the Alphafold2 predicted structure database identified SERTA domain proteins as high-confidence PP2A/B55α-binding structural homologs of IER5-N50. These studies define the molecular basis of PP2A/B55α inhibition by IER5-family proteins and suggest a roadmap for selective pharmacologic modulation of PP2A/B55α complexes.

36 **INTRODUCTION**

37 PP2A serine/threonine protein phosphatases are assembled from a scaffolding subunit (A, A'),
38 a catalytic subunit (C, C') and a regulatory subunit derived from one of four different protein
39 subfamilies (B/B55, B'/B56, B''/PR48-PR70, and B'''/striatin)[1]. The B55α form of PP2A
40 (PP2A/B55α) has critical roles in cell cycle regulation, mitotic exit, and the DNA damage
41 response[2–6]. In addition, the PP2A A-C subcomplex is also incorporated into the INTAC
42 submodule of the integrator complex, a transcriptional regulator[7,8].

43

44 A structure of PP2A/B55α bound to microcystin-LR defined the architecture of the heterotrimer
45 and showed how microcystin-LR inhibits dephosphorylation of pTau by binding to the active
46 site of the catalytic subunit [9]. FAM122A and ARPP19, proteins that regulate cell cycle
47 progression by selectively inhibiting PP2A/B55α[10–14], both engage the heterotrimer using a
48 bipartite binding interface in structures determined by single particle electron cryomicroscopy
49 (cryo-EM), contacting both a B55α surface and the catalytic subunit at the active site[11].

50

51 IER5 is a member of the AP1-regulated immediate early response (IER) gene family[15],
52 encoding a protein of 327 amino acids. *IER5* is induced in response to ionizing radiation and
53 is implicated in the cellular response to DNA damaging agents and heat shock[16–18]. In
54 squamous cell carcinoma (SCC) cells, *IER5* is a direct transcriptional target of activated Notch
55 that is required for induction of a cell differentiation program that arrests cell growth and
56 stimulates expression of *KRT1* and other keratinocyte-associated genes[19].

57

58 IER5 executes its cellular function, at least in part, by binding to and modulating the activity of
59 heterotrimeric B55α holoenzyme complexes of PP2A[19–22]. One model for IER5 function
60 proposes that it acts to direct selection of PP2A substrates such as S6K and HSF1 for

61 dephosphorylation[22]; however, in SCC cells, IER5 induction of gene transcription is mediated
62 by suppression of PP2A/B55α activity, suggesting an alternative model where IER5 functions
63 to antagonize PP2A activity against at least a subset of substrates[19].

64

65 Here, we report the structure of a PP2A/B55α in complex with the N-terminal domain of IER5
66 (IER5-N50), thereby uncovering the molecular basis of IER5's ability to inhibit PP2A/B55α.
67 Furthermore, using bioinformatics, we identify SERTADs as structural homologs of IER5-N50,
68 pointing to the existence of a larger family of PP2A/B55α regulatory proteins. Our novel
69 PP2A/B55α IER5-N50 structure identifies a strategy for selective modulation of PP2A/B55α
70 activity.

71

72 **RESULTS**

73 *Structure of a PP2A/B55α complex with IER5-N50.* Previous work demonstrated that the 50-
74 residue N-terminal domain of IER5 (IER5-N50), predicted to be a helical hairpin by Alphafold2
75 (Fig. S1A,B, related to Fig. 1), is necessary and sufficient for binding to PP2A/B55α, whereas
76 the C-terminal region (IER5-C) of IER5, predicted to be unstructured (Fig. S1A, related to Fig.
77 1), does not interact[19]. To elucidate the molecular basis for IER5 recruitment to PP2A/B55α,
78 we expressed and purified a complex of PP2A/B55α with IER5-N50 (Fig. S1C related to Fig.
79 1) and determined its structure using cryo-EM (Fig. 1 and Figs. S2 and S3, related to Fig. 1).
80 During data processing, we observed that the complexes existed in monomeric and dimeric
81 assemblies (Fig. S2, related to Fig. 1). We utilized both assemblies during data processing
82 and determined a final map of the monomeric assembly with a global resolution of 3.27 Å
83 (Table 1, Figs. 1A, 1B and Fig. S3, related to Fig. 1). In complex with IER5-N50, the curvature
84 of the A subunit of the PP2A heterotrimer is increased compared to that of PP2A-B55α in the
85 structure with bound microcystin-L (PDB:3DW8[9], Fig. S4A, related to Fig. 1), and similar to
86 that seen in PP2A complexes with FAM122A and ARPP19 (Fig. S4B, related to Fig. 1). We

87 thus used the structure of PP2A-B55α in complex with FAM122A (PDB:8SO0[11]) as an initial
88 model in building the PP2A heterotrimer in the IER5 complex. IER5 residues 3-45 were then
89 built into the unmodelled region of the map adjacent to B55α using an initial model of IER5-
90 N50 derived from Alphafold2[23] (Fig. S1A, related to Fig. 1). In the final refined model (Fig. 1A),
91 the RMSD of the PP2A/B55α portion of the model for the IER5 complex has values of 1.4 Å
92 and 1.5 Å when compared to the FAM122A and ARPP19 complexes, respectively (Fig. S4B)[11].

93

94 IER5-N50 adopts a helical hairpin conformation in the complex, forming an extensive contact
95 interface with B55α to bury a total surface area of 2381 $Å^2$ (Fig. 1C). In contrast to FAM122A
96 and ARPP19, which contact both B55α and the catalytic subunit of PP2A[11], IER5-N50 only
97 contacts B55α (Fig. S4B, related to Fig. 1). There is electrostatic complementarity between
98 the B55α binding surface, which contains acidic patches on its top face, and the binding
99 surface of IER5, which is largely basic (Fig. 1D).

100

101 The contact interface on B55α derives from the exposed face of its beta propeller, which
102 presents a trio of short helices and a series of four extended loops to create a groove with two
103 interaction sites for IER5 (Fig. 2A). At the first site, the helices of B55α engage the two helices
104 of IER5 using contacts that are predominantly hydrophobic, with residues F281, I284, Y337,
105 and F343 of B55α packing against I10, I13, L35, V36, and V39 of IER5 (Fig. 2B, left). S14
106 intramolecularly bridges the two helices of IER5 by reaching within hydrogen bonding distance
107 of the backbone carbonyl of V39. The side chain of Y337 on B55α sits centrally in this surface,
108 with its hydroxyl group approaching within hydrogen bonding distance of the backbone
109 carbonyl of V36. Additionally, there are electrostatic contacts between the side chains of E338
110 from B55α and R9 of IER5, and between the K17 side chain of IER5 and the backbone
111 carbonyls of Y337 and E338 of B55α. At the N-terminal end of IER5 helix 2, L30 and L34 pack
112 in a hydrophobic cluster with M222, L225, and V228 of B55α (Fig. 2B, right). H31 and K32

113 impart a positive electrostatic surface for interaction with the acidic platform of B55α, with the
114 IER5 H31 side chain coming within hydrogen bonding distance of K345 on B55α.

115

116 The second site on B55α is derived from the loops connecting adjacent beta strands of the
117 propeller, which present an acidic surface to the basic loop of IER5 that connects its helices
118 (Fig. 2C). This segment of IER5 resembles a Short Linear Motif (SLiM)[24], with a side chain
119 electrostatic interaction between R25 and E93 of B55α. The R25 side chain is also within
120 hydrogen bond distance of the backbone carbonyls of E91 and I92 on B55α, and the K29 side
121 chain amino group is positioned to form a salt bridge with the carboxyl group of D116 from
122 B55α. H179 of B55α also approaches within hydrogen bonding distance of the K29 amino
123 group.

124

125 *Validation of the binding interface.* To test the importance of the hydrophobic and electrostatic
126 surfaces of IER5-N50 in formation of complexes with PP2A/B55α, we introduced single point
127 mutations into full-length IER5 (IER5-FL) at B55α interface residues or at control sites (L15
128 and N20) distant from the contact interface and tested their effects on B55α co-
129 immunoprecipitation in IER5 knockout cells (Fig. 2D). Wild-type IER5, the IER5 L15R mutant,
130 and the N20A mutant all strongly co-immunoprecipitated B55α. In contrast, interface mutations
131 either completely prevented (S14A, K17E, L30E) or greatly reduced (I10A, R25E, K29E,
132 H31A, K32E, L35A, V39A) co-immunoprecipitation of B55α, confirming that the interface seen
133 in the cryo-EM structure is required for binding of IER5-FL to B55α in cells.

134

135 *IER5 inhibits PP2A dephosphorylation of pTau.* The region of PP2A/B55α bound by IER5-N50
136 overlaps with residues required for recruitment of a broad set of substrates to PP2A/B55α[9,25,26]
137 (Fig. S4C, related to Fig. 3). To investigate the effect of IER5 on PP2A/B55α substrate
138 dephosphorylation, we purified the PP2A/B55α holoenzyme, FLAG-tagged MBP fusions of

139 IER5-N50 and full-length IER5 (IER5-FL), and FLAG-tagged MBP fusions of IER5-N50 and
140 IER5-FL with the K17E mutation (Fig. S5, related to Fig. 3). Using pTau as a substrate[9], we
141 compared the inhibitory activity of these proteins with that of FAM122A, a known PP2A/B55α
142 inhibitor[10,11,14] (Fig. 3A-C). Both IER5-FL (IC50, 2.2 μM) and IER5-N50 (IC50, 2.3 μM) MBP
143 fusion proteins inhibited pTau dephosphorylation by PP2A/B55α similarly to each other and to
144 FAM122A (IC50, 3.1 μM) (Fig. 3). In contrast, the K17E mutated forms of IER5-FL and IER5-
145 N50 failed to inhibit pTau dephosphorylation (Fig. 3), confirming that IER5 inhibition of
146 PP2A/B55α requires complex formation.

147

148 *Determining the minimal molecular requirements of IER5 essential for KRT1 transcription.* In
149 the SCC cell line SC2, IER5 is necessary for Notch-dependent induction of *KRT1* expression
150 (Fig. 4A), a requirement that is relieved when B55α is knocked out and restored when wild-
151 type IER5-FL is reintroduced into IER5 knockout, B55α wild-type SC2 cells[19]. Reintroduction
152 of either the L15R or N20A mutant of IER5-FL, neither of which disrupt recovery of B55α in
153 the co-immunoprecipitation assay (Fig. 2D), rescues expression of KRT1 in response to Notch
154 activation comparably to IER5-FL, whereas IER5-FL variants harboring an I10A, S14A, K17E,
155 or L30E interface disrupting mutation all greatly reduce *KRT1* expression, as determined by
156 RT-qPCR (Fig. 4B). These data show that interfering with the binding of IER5 to B55α leads
157 to a loss of IER5 function in SC2 cells.

158

159 We next performed structure-function studies to determine the minimal molecular
160 requirements for IER5 rescue of *KRT1* expression (Fig. 4). IER5-N50 did not restore *KRT1*
161 expression, showing that PP2A binding activity is insufficient for inhibitory function in cells, and
162 IER5-C also failed to rescue *KRT1* expression (Fig. 4C-E). In contrast, serial truncations and
163 internal deletions within the IER5-C region showed that IER5-N50 region and the C-terminal

164 bipartite nuclear localization sequence[27] were sufficient for induction of *KRT1* expression (Fig.
165 4F-K).

166

167 *Identification of IER5-N50 homology to SERTA domain containing proteins.* We next queried
168 the entire human alphafold-predicted proteome using Foldseek[28] to determine if any other
169 proteins are predicted to contain a helical hairpin domain related to that of IER5-N50. Among
170 the top hits were SRTD2 and CDCA4 (Probability 0.9 and 0.82, respectively) (Fig. 5A, B),
171 proteins belonging to a larger family of SERTA domain-containing (SERTAD) proteins
172 previously implicated as PP2A/B55α-binding proteins[29,30]. Notably, the positions on IER5 that
173 are essential for PP2A/B55α binding are among the most conserved residues in the
174 IER/SERTAD protein superfamily (Fig. 5B, red dots). Based on structure-based sequence
175 alignment, there are consensus motifs of ([I/L][F/W]XFSFXKF) in helix 1, and
176 ([H/K/R]XXL[L/I]X[S/N]) in helix 2 (with aliphatic and aromatic residues denoted as F or W,
177 respectively; Fig. 5C). Interestingly, the loop of IER5, which is analogous to a SLiM[24] on other
178 PP2A-binding proteins, is more poorly conserved. Structures of complexes between
179 PP2A/B55α and SERTAD proteins are predicted with high-confidence scores using alphafold
180 multimer[31,32] (Fig. 5D and Table S1, related to Fig. 5). This analysis strongly suggests that
181 IER5 is representative of a broader superfamily of proteins that modulate PP2A/B55α function
182 by binding to B55α using a helical hairpin motif.

183

184

185 **DISCUSSION**

186 The PP2A phosphatase utilizes a set of regulatory subunits, including B55α, to maintain
187 cellular homeostasis by specifically recruiting substrates for dephosphorylation in response to
188 cellular signaling cues. Modulators of PP2A/B55α activity, such as the inhibitors FAM122A and
189 ARPP19, have overlapping and distinct roles in cell cycle-specific control of PP2A/B55α
190 activity[10–14]. In previous work, we showed that IER5 is epistatic to B55α in the response to
191 Notch activation in SCC cells, in which *KRT1* expression, a marker of keratinocyte
192 differentiation, is dependent on Notch-induced expression of *IER5*[19].

193

194 The work reported here shows that the N-terminal helical hairpin of IER5 acts as an inhibitor
195 of PP2A/B55α phosphatase activity by occluding the substrate-binding platform of the B55α
196 regulatory subunit. IER5-N50 masks an extensive region on the surface of B55α that faces,
197 but does not directly contact, the catalytic subunit (Figs. 1, 2). Substrate recruitment to B55α
198 relies primarily on short linear motifs (SLiMs), which may adopt an alpha helical conformation
199 when bound[24,25]. Residues on B55α reported to participate in substrate recruitment and
200 function show substantial overlap with the IER5 binding site[9,25,26] (Fig. S4C), consistent with
201 our findings that IER5-FL and IER5-N50 inhibit PP2A/B55α pTau dephosphorylation (Fig. 3).
202 The mode of IER5 binding differs from that of the PP2A inhibitors FAM122A and ARPP19,
203 which both engage the B55α subunit with a short helical motif and contact the catalytic subunit
204 using a discontinuous unstructured segment[11,14] (Fig. S4B)**.** The more closed conformation of
205 the PP2A-IER5 complex, as compared to the microcystin-L-inhibited structure[9], also allows
206 the B55α regulatory subunit to contact the C-terminal tail of the catalytic domain directly (Fig.
207 S4, related to Fig. 1).

208

209 Others have proposed that IER5 functions as a substrate adaptor, enabling PP2A to
210 dephosphorylate proteins that do not bind B55α directly[22]. Though the findings reported here

211 disfavor this possibility, they do not exclude the possibility that loading of IER5 onto
212 PP2A/B55α complexes could inhibit dephosphorylation of some substrates while promoting
213 dephosphorylation of other proteins.

214

215 IER5 function appears to require both B55α binding and nuclear entry, because IER5 does
216 not restore the expression of *KRT1* in IER5 knockout cells unless the N50 module and its
217 bipartite nuclear localization sequence[27] are both present (Fig. 4). By mining the alphafold
218 predicted human proteome with a structure similarity search[28], we also found that IER5 is likely
219 representative of a larger protein superfamily that regulates PP2A/B55α by using a helix-loop-
220 helix motif to recognize B55α. Among these helix-loop-helix containing proteins are the
221 SERTADs, for which a functional link to PP2A/B55α has already been established[29,30]. Other
222 studies have shown that SERTAD proteins contain potent transcriptional activation domains[33–
223 36], and recent work has also suggested that IER5 has activity as a transcriptional regulator[20].
224 How the transcriptional regulatory activity of IER5 relates to its activity as a selective inhibitor
225 of nuclear PP2A/B55α complexes and whether this is a property shared with SERTADs and
226 other helix-loop-helix superfamily members should be fertile ground for future studies.

227

228 The immediate early response genes also include a family member called IER3 (also known
229 as IEX-1), which is closely related to IER5. IER3 does not bind B55α and instead inhibits the
230 activity of the PP2A/B56 isoform by promoting the dissociation of B56 from the active
231 enzyme[37,38]. Of interest, *IER3* also appears to be a direct target of Notch signaling in SCC
232 cells[19]. The induction of different immediate early response proteins by Notch and cell stresses
233 such as radiation-induced DNA damage may serve to induce cell cycle arrest and
234 differentiation of squamous cells through the coordinated inhibition of multiple PP2A
235 holoenzyme species.

236

237 Lastly, there is interest in development of PP2A modulators for diseases ranging from
238 neurodegeneration to cancer[39,40]. The molecularly distinct IER5 contact site identified here
239 could serve as a target surface for developing protein-protein interaction (PPI) inhibitors that
240 selectively block substrate recruitment to PP2A/B55α complexes, or conversely, for molecular
241 glue modulators that can direct dephosphorylation of specific proteins, analogous to protein-
242 degrading IMiDs[41].

243

244 **ACKNOWLEDGMENTS**

245 We thank the Cryo-EM Center for Structural Biology at Harvard Medical School for help and
246 advice with data collection, and members of the Blacklow lab and Alan Brown for helpful
247 discussions. We thank Ernst Schmid for running and scoring alphafold predictions. This work
248 was supported by NIH awards 1R35 CA220340 (to SCB) and 1R01 CA272484 (to SCB), the
249 Ludwig Center at Harvard (JCA), the Warren Alpert Foundation (to SCB), and the Blavatnik
250 Institute of Harvard Medical School.

251

252 **AUTHOR CONTRIBUTIONS**

253 JCA and SCB conceived the project and acquired funding. RC purified PP2A/B55α-IER5
254 complexes, acquired biochemical data, prepared samples for cryo-EM data collection, and
255 collected cryo-EM images. SKRP provided purified FAM122A protein. DTDJ processed and
256 analyzed cryo-EM data with input from SR and RC, and DTDJ built the structural models with
257 input from SCB and RC. LP performed co-immunoprecipitation studies and *KRT1* expression
258 analyses. All authors participated in data analysis and interpretation. SCB, RC, DTDJ, and
259 JCA wrote and edited the manuscript with input from all authors. All authors agreed on the
260 final manuscript.

261

262 **COMPETING INTERESTS STATEMENT**

263 SCB is on the board of directors of the non-profit Institute for Protein Innovation and the
264 Revson Foundation, is on the scientific advisory board for and receives funding from Erasca,
265 Inc. for an unrelated project, is an advisor to MPM Capital, and is a consultant for IFM,
266 Scorpion Therapeutics, Odyssey Therapeutics, Droia Ventures, and Ayala Pharmaceuticals
267 for unrelated projects. JCA is a consultant for Ayala Pharmaceuticals, Cellestia, Inc.,
268 SpringWorks Therapeutics, and Remix Therapeutics. The other authors declare that they have
269 no competing interests.

270

271 **METHODS**

272 **Plasmid construction**

273 cDNAs encoding PPP2R1A, PPP2CA, and PPP2R2A (B55α) assembled in a pAC-derived
274 baculovirus expression vector (pAC8RedNK) were gifts from the Fischer lab (Dana Farber
275 Cancer Institute). PPP2R1A was engineered to include an N-terminal His_6 tag followed by a
276 Tobacco etch virus (TEV) cleavage site; the cDNA for PPP2R2A (B55α) had no affinity tag;
277 and PPP2CA had an N-terminal Flag tag followed by a TEV cleavage site. The IER5 (1-50)
278 fragment was subcloned into pAC8RedNK with an N-terminal Strep tag II followed by a TEV
279 cleavage site. Both the IER5 (1-50) and full length IER5 were cloned into the
280 pcDNA3.1/hygro(+) vector with an N-terminal Flag-MBP tag followed by a TEV cleavage site.
281 K17E mutations of IER5 proteins were made using site-directed mutagenesis. The full-length
282 Tau protein was cloned into the bacterial expression vector ptd68, incorporating an N-terminal
283 His_6-SUMO tag. Insert sequences were confirmed by Sanger sequencing.

284

285

286 **Protein Expression**

287 The PP2A/B55α heterotrimer and the PP2A/B55α IER5-N50 complex were expressed in Hi5
288 cells by concurrently transfecting 1.5 µg of the pAC8RedNK vector and 0.5 µg of linearized
289 baculoviral DNA into $1x10^6$ Sf9 cells using 6 µl of FuGene HD (Promega) in ESF 921 Insect
290 Cell Culture medium (Expression Systems). After 5 to 7 days of incubation, the supernatant
291 was collected to harvest the baculovirus. The virus was subsequently amplified over 2 to 3
292 cycles using Sf9 cells at a concentration of $2x10^6$. The collected viruses were then used to
293 infect Hi5 cells for protein expression. For expression of the PP2A heterotrimer, a viral
294 stoichiometric ratio of 1:1:1 was used for Hi5 cell infection. For the PP2A-IER5 complex, a
295 ratio of 1:1:1:1.5 (IER5) was used. Cells were shaken at 27 °C for 72 hours before harvesting
296 by centrifugation. Cell pellets were collected and stored at −80 °C until purification.

297

298 Flag-MBP-IER5-N50 and Flag-MBP-IER5-FL protein were expressed in Expi293F cells. Cells
299 were grown in Expi293 media to a density of 3×10^6 cells/ml and then transfected with 1.0 mg
300 DNA/L of culture using the FectroPro transfection reagent (Polyplus) at a 1:1 DNA/FectroPro
301 ratio. After 24 hours, 45% D-(+)-Glucose solution (Sigma-Aldrich, 10 mL per L of culture) and
302 3 mM valproic acid sodium salt (Sigma-Aldrich) were added to the cells to enhance protein
303 expression. The cells were cultured for an additional 24 hours before harvesting by
304 centrifugation. Cell pellets were collected and stored at −80 °C until purification.

305

306 Recombinant Tau protein was expressed in E. coli BL21 (DE3) cells. Protein expression was
307 induced at a culture optical density (OD) of 0.8 by addition of 0.2 mM isopropyl-1-thio-D-
308 galactopyranoside (IPTG) and the culture was maintained at 16°C overnight. Cell pellets were
309 collected and stored at −80 °C until purification. Recombinant FAM122A was expressed and
310 purified as reported[11].

311

312 **Protein purification**

313 For the PP2A heterotrimer, cells were resuspended in lysis buffer containing 20mM Tris-HCl,
314 pH 7.6, 200mM NaCl, 2mM Tris-(2-carboxyethyl) phosphine (TCEP), 0.1% (v/v) Triton X-100,
315 protease inhibitor cocktail (Sigma) and Benzonase (EMD Millipore). Cells were lysed by
316 sonication and centrifuged at 50,000 *g* for 1 h. The soluble fraction was passed over an anti-
317 FLAG M2 affinity resin. The resin was washed with 10 column volumes (CVs) of wash buffer
318 (20 mM Tris-HCl, pH 7.6, 200 mM NaCl, 2 mM TCEP), and the protein was then eluted using
319 wash buffer supplemented with 0.2 mg/ml of FLAG peptide. The elution fractions were
320 collected, concentrated, and further purified using size-exclusion chromatography (SEC) on a
321 Superdex S200 10/300 column, which was pre-equilibrated with buffer (20 mM Tris-HCl, pH
322 7.6, 200 mM NaCl, 2 mM TCEP). Protein purity was assessed by SDS-PAGE using a
323 Coomassie blue stain. Peak fractions were pooled for biochemical studies.

324

325 For the PP2A/B55-IER5 complex, lysis and ultracentrifugation were performed as above. The
326 affinity purification step was performed using Strep-Tactin XT Superflow resin (IBA), followed
327 by elution with wash buffer supplemented with 50 μM biotin. After elution from the column the
328 fractions were concentrated and further purified using size exclusion chromatography on a
329 Superdex S200 10/300 column. Protein purity was assessed by SDS-PAGE using a
330 Coomassie blue stain. Peak fractions were pooled for biochemical studies and for Cryo-EM
331 data collection.

332

333 For purification of IER5 proteins, cells were resuspended in lysis buffer containing 20mM Tris-
334 HCl, pH 7.6, 200mM NaCl, 2mM Tris-(2-carboxyethyl) phosphine (TCEP), protease inhibitor
335 cocktail (Sigma) and Benzonase (EMD Millipore). Cells were lysed by sonication and
336 centrifuged at 50,000 *g* for 1 h. The soluble fraction was passed over amylose resin. The resin
337 was washed with 10 column volumes (CVs) of wash buffer (20 mM Tris-HCl, pH 7.6, 200 mM

338 NaCl, 2 mM TCEP), 50 CVs of wash buffer supplied with 10mM Mgcl2, 5mM ATP, and 5CVs
339 of wash buffer, and the protein was then eluted using wash buffer supplemented with 10 mM
340 maltose. The elution fractions were collected, concentrated, and further purified using size-
341 exclusion chromatography (SEC) on a Superdex S200 10/300 column, which was pre-
342 equilibrated with buffer (20 mM Tris-HCl, pH 7.6, 100 mM NaCl, 2 mM TCEP). Protein purity
343 was assessed by SDS-PAGE using a Coomassie blue stain. Peak fractions were pooled for
344 biochemical studies.

345

346 For preparation of Tau protein, bacterial cells were resuspended in lysis buffer containing 20
347 mM Tris-HCl, pH 8, 200 mM NaCl, 2 mM Tris-(2-carboxyethyl) phosphine (TCEP), protease
348 inhibitor cocktail (Sigma), 20 mM Imidazole. Cells were lysed by sonication and centrifuged to
349 remove debris. After centrifugation, the supernatant containing the recombinant His-SUMO-
350 Tau was applied to Ni(NTA) affinity resin, and the resin was washed using lysis buffer. The
351 His-SUMO tag was removed overnight by on-column cleavage with ULP1 protease. Protease-
352 liberated Tau was recovered from the column flow-through and was further purified by size
353 exclusion chromatography using a Superdex 75 10/300 GL (GE Healthcare) column in buffer
354 consisting of 20 mM Tris-HCl pH 8, 200 mM NaCl, and 2mM TCEP. Peak fractions were pooled
355 for phosphorylation using GSK3β. The concentration of purified Tau was determined by UV
356 absorbance at 280 nm.

357

358 **Phosphorylation of Tau protein and purification of pTau**

359 Purified Tau was incubated with GSK3β (SinoBiological) in a 100:1 ratio, using a buffer of 25
360 mM HEPES pH 7.5, containing 100 mM NaCl, 10 mM $MgCl_2$, 10 mM ATP, and 2 mM TCEP.
361 The reaction was allowed to proceed for 19 hours at 37 ^{o}C. Verification that the reaction had
362 gone to completion was performed by SDS-PAGE with Coomassie blue staining. The pTau
363 was further purified by size exclusion chromatography using a Superdex 75 10/300 GL (GE

364 Healthcare) column in buffer consisting of 20 mM Tris-HCl pH 8, 200 mM NaCl, and 2mM
365 TCEP. The concentration of purified pTau was determined by UV absorbance at 280 nm.
366 Fractions were collected and frozen in -80 prior to use.

367

368 **Cryo-EM grid preparation and data collection**

369 Samples were frozen on Cryo-EM grids using a Vitrobot Mark IV (Thermo Fisher Scientific)
370 instrument for vitrification. Freshly purified PP2A-IER5 complex (3.5 µl at a concentration of 2
371 mg/ml) was deposited onto glow-discharged C-flat holey carbon grids (R1.2/1.3, 400 mesh
372 copper, Electron Microscopy Sciences). These grids were blotted for 6 seconds with a blot
373 force of 15 at 100% humidity and 22 ^{o}C before being rapidly submerged into liquid nitrogen-
374 cooled liquid ethane.

375

376 Images were acquired on a Titan Krios microscope equipped with a BioQuantum K3 Imaging
377 Filter (slit width 25 eV) and a K3 direct electron detector (Gatan), operating at an acceleration
378 voltage of 300 kV. Images were recorded at a defocus range of −0.8 to −2.0 µm with a nominal
379 magnification of 105 kx, resulting in a pixel size of 0.825 Å. Each image was dose fractionated
380 into 51 movie frames with a total exposure time of 2.8 s, resulting in a total dose of ~53.7
381 electrons per Å^2. SerialEM was used for data collection.

382

383 **Structure Determination**

384 Data were processed using CryoSPARC[42] unless explicitly stated in the text, as summarized
385 in Fig. S3. A total of 5,383 micrographs were subjected to patch motion correction and patch
386 CTF estimation. Particles (3.95 million) were identified and extracted using a box size of 360
387 pixels using the CryoSPARC blob picker. 2D-classification was used to remove poorly
388 classified particles, reducing the total number of particles to 1.17 million. From the projected

389 2D-class averages, a mixture of monomeric and dimeric PP2A-IER5 assemblies was evident.
390 100k particles were split and used to generate three preliminary maps representing the
391 different species present in the data. The three maps were subjected to heterogeneous
392 refinement using all identified particles, resulting in three classes designated as monomeric
393 (~47%), dimeric (~25%) and junk (~27%) (e.g., scaffolding subunit only) classes. The
394 monomeric and dimeric classes were then processed independently. Non-uniform refinement,
395 local motion correction, and another round of non-uniform refinement was applied to the
396 monomer class, yielding a map with a nominal resolution of 3.67 Å. The monomer class
397 displayed no clear IER5 density at this stage of processing. Non-uniform refinement, local
398 motion correction, and another round of non-uniform refinement was applied to the dimeric
399 class, resulting in a resolution of 3.67 Å for the dimer class map. Alignment of the dimeric map
400 along an apparent C2 symmetry axis followed by non-uniform refinement under a C2
401 symmetry constraint improved the map to 3.44 Å resolution. A further round of local motion
402 correction and two rounds of sequential non-uniform refinement produced a map of 3.17 Å
403 resolution. Symmetry expansion was performed along the C2 symmetry axis. Masked local
404 refinement with a soft mask (shown in black outline box named “local refinement mask”)
405 around a single copy from an asymmetric unit produced a map at 3.04 Å resolution. Despite
406 this reasonable global resolution, the map displayed strong directional anisotropy.

407

408 Masked non-uniform refinement using a single copy of an asymmetric unit of the symmetry
409 expanded dimer map, using the monomeric particles as input, resulted in a 3.82 Å map with
410 improved signal for IER5. We then combined all the aligned monomer and symmetry
411 expanded dimer particles and performed a masked local refinement that resulted in a
412 combined map of 3.09 Å resolution. To resolve conformational heterogeneity in IER5 we
413 generated a mask around IER5 only and performed masked 3D classification without
414 alignment in Relion[43] (K = 4, T = 20). Once particle class convergence was reached, a single
415 class contained the majority particles (60.1 %) and displayed high resolution features. Further

416 3D classification was ineffective at improving map quality, we therefore utilised CryoSieve[44]
417 with reconstruction in Relion and reduced the particle stack to ~99k particles without impacting
418 the quality of IER5 (nominal resolution of 3.14 Å).

419

420 We then made a mask on the alternate copy of PP2A/B55α-IER5, attributed by the dimer
421 particles of PP2A/B55, and performed a local refinement on this copy[45]. Using the same mask,
422 we then performed particle subtraction on this copy of PP2A/B55α-IER5 from the map. Using
423 the particle subtracted stack and the alignments from the CryoSieved map reconstruction as
424 input, we performed a local refinement around the previously refined copy of PP2A/B55α-
425 IER5, reaching 3.18 Å resolution. In the previous step we determined the per particle input
426 scale during local refinement, and used the score with the rebalance orientations job in
427 cryosparc, reducing to a final particle stack of 67k particles with a nominal resolution of 3.27
428 Å. We post-processed the output half maps using DeepEMhancer[46], and used this map to aid
429 inspection, manual model building, and visual illustration.

430

431 **Model refinement and atomic model building**

432 We used the PP2A/B55α-FAM122A structure (PDB 8SO0[11]) as an initial model for the PP2A/
433 B55α heterotrimer, and an initial model for IER5 as predicted by alphafold[23]. The models were
434 fitted to the map by hand using Chimerax[47]. The model fit to the map was improved using
435 ISOLDE and adaptive distance constraints to maintain local geometries and distances when
436 applicable[48]. The model was refined iteratively using REFMAC Servalcat[49] and Phenix Real-
437 Space Refine[50]. During refinement in REFMAC Servalcat or manual refinement in Coot,
438 positional restraints generated using ProSMART[51] were used. The final models were
439 evaluated using MolProbity[52] in Phenix validation report. Statistics of the map reconstruction
440 and model refinement are presented in Extended Data Table 1 and taken from Phenix
441 validation report. Structural biology applications used in this project (except CryoSPARC) were

442 compiled and configured by SBGrid[53]. Molecular graphics and analyses were performed with
443 UCSF ChimeraX[47] (developed by the Resource for Biocomputing, Visualization, and
444 Informatics at the University of California, San Francisco, with support from National Institutes
445 of Health R01-GM129325 and the Office of Cyber Infrastructure and Computational Biology,
446 National Institute of Allergy and Infectious Diseases), or PyMOL (Schrödinger).

447

448 **Enzymatic analysis of dephosphorylation of pTau *in vitro***

449 PP2A/B55α holoenzyme in enzyme buffer (20 mM Tris pH 7.6, 100 mM NaCl, 2 mM TCEP)
450 was pre-incubated with various concentrations of IER5-N50, IER5-FL, IER5-N50 variants,
451 IER5-FL variants, or FAM122A for 2 h on ice. The reaction was started by adding pTau (final
452 concentration 0.35 μM) to the PP2A/B55α - inhibitor complexes (final concentration of
453 PP2A/B55α holoenzyme, 20 nM) and incubating at 30 °C. After 30 min, the reaction was
454 stopped by adding SDS loading buffer and the samples were loaded onto SDS-PAGE. The
455 phosphorylation status of Tau was examined by western blot using an antibody (Thermo
456 Scientific) that specifically recognizes phosphorylated serine 396 of Tau. The experiments
457 were independently repeated at least 3 times ($n \geq 3$).

458

459 **Cell culture**

460 Cells were grown under 5% CO2 at 37°C in media supplemented with streptomycin/penicillin.
461 IER5 knock-out cell line I5 was derived from SC2 cells, which are engineered to contain a
462 cDNA encoding a mutated truncated form of NOTCH1, ΔEGF-L1596H, that is regulatable with
463 a γ-secretase inhibitor (GSI)[19]. I5 and its derivatives overexpressing wide-type or mutant IER5
464 were cultured in keratinocyte medium as described[54] in the presence of GSI (1 μM compound
465 E) to maintain Notch in the off-state. Timed activation of Notch was triggered by GSI washout
466 as described[19].

467 **Expression Constructs, Viral Production and Infection of Cells**

468 The expression vector MIEG3-IER5-FH was constructed by inserting human IER5 tagged with
469 HA and 3XFLAG into the MIEG3 vector[19], which is a murine stem cell virus (MSCV)-based
470 bicistronic retroviral construct expressing EGFP. MIEG3 expression plasmids containing IER5
471 and variants with point mutations were generated using a QuickChange II Site-Directed
472 Mutagenesis Kit (Agilent). MIEG3 expression plasmids containing deletional IER5 mutants
473 were constructed by replacing full-length IER5 in MIEG3-IER5-FH with PCR-generated DNA
474 fragments containing mutant forms of IER5. Retrovirus was prepared by transfecting Phoenix-
475 gp cells with the MIEG3 vector and expression vectors for Gag/Pol and GALV. Viral
476 supernatant was collected 48 h after transfection, centrifuged, and filtered through a 0.45 μm
477 filter (Corning). For infection of target cells, 1 ml of virus was mixed with cells and protamine
478 sulfate in a 6-well plate, and the plate was then centrifuged at 2,250 rpm for 90 min at room
479 temperature. GFP-expressing cells were then isolated by cell-sorting several days after
480 transduction as described[19].

481

482 **Quantitative RT-PCR**

483 After 72 hours of GSI washout, cells were resuspended in Trizol (Life Technologies) and total
484 RNA was prepared with RNeasy Mini kit (Qiagen). cDNA was synthesized with High-Capacity
485 cDNA Reverse Transcripition Kit (Applied Biosystems). PCR was performed using the
486 PowerUP SYBR Green Master Mix (Applied Biosystems) with QuantStudio 3 Real-Time PCR
487 System (Applied Biosystems). Primers used for *KRT1* and *GAPDH* are: forward 5'-
488 GGACAGCTCCTTAGCATCTTATC-3', reverse 5'-GGAGTTTAAGACCTCTCCACAAA-3', and
489 forward 5'-GAAGGTGAAGGTCGGAGTCAAC-3', reverse 5'-
490 TGGAAGATGGTGATGGGATTTC-3', respectively.

491

492 **Immunoprecipitation and Western Blotting**

493 For immunoprecipitation assays, cells in 10-cm dishes were washed in cold PBS and lysed in
494 1 ml of Pierce IP Lysis Buffer (Thermo Scientific) supplemented with protease inhibitors
495 (Sigma). Cell lysates with equal amounts of protein were incubated with 25μl of washed Pierce
496 Anti-HA Magnetic Beads (Thermo Scientific) overnight at 4°C with mixing. The beads were
497 then washed three times with TBS-T and once with ultrapure water. The HA-tagged IER5 and
498 its associated proteins were eluted with Pierce HA peptide (Themo Scientific). The eluates
499 and input proteins were loaded on 3-8% SDS-polyacrylamide gels and resolved by
500 electrophoresis. Following transfer to nitrocellulose membranes, proteins were incubated at
501 4° C overnight with the following primary antibodies: anti-PP2A B55 (100C1) or anti-HA
502 (C29F4) (both from Cell Signaling Technology); or anti-IER5 (HPA029894) or anti-Flag
503 (F3165) (both from Sigma). Secondary antibody was either goat anti-rabbit (7074) or horse
504 anti-mouse (7076) IgG conjugated with horseradish peroxidase (Cell Signaling Technology).
505 Staining was developed with SuperSignal West Dura Extended Duration Substrate (Thermo
506 Scientific) for 2min at room temperature and documented by exposure to x-ray film.

507

508 **Statistical analysis**

509 Statistical analysis was performed using GraphPad Prism version 10 (GraphPad). Statistical
510 details are indicated in the Figure Legends. Sample distribution and normality tests were
511 performed for each data set and significance was determined using Welch's t test.

512

513

REFERENCES

1. Amin, P. *et al.* PP2A-B55: substrates and regulators in the control of cellular functions. *Oncogene 2021 41:1* **41**, 1–14 (2021).
2. Grallert, A. *et al.* A PP1/PP2A phosphatase relay controls mitotic progression. *Nature* **517**, 94 (2015).
3. Krasinska, L. *et al.* Protein phosphatase 2A controls the order and dynamics of cell-cycle transitions. *Molecular cell* **44**, 437–450 (2011).
4. Swartz, S. Z. *et al.* Selective dephosphorylation by pp2a-b55 directs the meiosis i-meiosis ii transition in oocytes. *eLife* **10**, (2021).
5. Wurzenberger, C. & Gerlich, D. W. Phosphatases: providing safe passage through mitotic exit. *Nature Reviews Molecular Cell Biology 2011 12:8* **12**, 469–482 (2011).
6. Schmitz, M. H. A. *et al.* Live-cell imaging RNAi screen identifies PP2A–B55α and importin-β1 as key mitotic exit regulators in human cells. *Nature Cell Biology 2010 12:9* **12**, 886–893 (2010).
7. Huang, K. L. *et al.* Integrator Recruits Protein Phosphatase 2A to Prevent Pause Release and Facilitate Transcription Termination. *Molecular cell* **80**, 345 (2020).
8. Zheng, H. *et al.* Identification of Integrator-PP2A complex (INTAC), an RNA polymerase II phosphatase. *Science* **370**, (2020).
9. Xu, Y., Chen, Y., Zhang, P., Jeffrey, P. D. & Shi, Y. Structure of a Protein Phosphatase 2A Holoenzyme: Insights into B55-Mediated Tau Dephosphorylation. *Molecular Cell* **31**, 873–885 (2008).
10. Fan, L. *et al.* FAM122A, a new endogenous inhibitor of protein phosphatase 2A. *Oncotarget* **7**, 63887–63900 (2016).
11. Padi, S. K. R. *et al.* Cryo-EM structures of PP2A:B55–FAM122A and PP2A:B55–ARPP19. *Nature 2023 625:7993* **625**, 195–203 (2023).
12. Gharbi-Ayachi, A. *et al.* The substrate of Greatwall kinase, Arpp19, controls mitosis by inhibiting protein phosphatase 2A. *Science* **330**, 1673–1677 (2010).
13. Mochida, S., Maslen, S. L., Skehel, M. & Hunt, T. Greatwall phosphorylates an inhibitor of protein phosphatase 2A that is essential for mitosis. *Science* **330**, 1670–1673 (2010).
14. Wasserman, J. S. *et al.* FAM122A ensures cell cycle interphase progression and checkpoint control by inhibiting B55α/PP2A through helical motifs. *Nature Communications 2024 15:1* **15**, 1–20 (2024).
15. Williams, M. *et al.* Ier5, a novel member of the slow-kinetics immediate-early genes. *Genomics* **55**, 327–334 (1999).
16. Ding, K. K. *et al.* Induced expression of the IER5 gene by γ-ray irradiation and its involvement in cell cycle checkpoint control and survival. *Radiation and Environmental Biophysics* **48**, 205–213 (2009).
17. Ishikawa, Y. & Sakurai, H. Heat-induced expression of the immediate-early gene IER5 and its involvement in the proliferation of heat-shocked cells. *The FEBS Journal* **282**, 332–340 (2015).
18. Kis, E. *et al.* Microarray analysis of radiation response genes in primary human fibroblasts. *International Journal of Radiation Oncology Biology Physics* **66**, 1506–1514 (2006).
19. Pan, L. *et al.* IER5, a dna damage response gene, is required for notch-mediated induction of squamous cell differentiation. *eLife* **9**, 1–32 (2020).
20. Asano, Y. *et al.* IER5 generates a novel hypo-phosphorylated active form of HSF1 and contributes to tumorigenesis. *Scientific Reports 2016 6:1* **6**, 1–19 (2016).
21. Ishikawa, Y., Kawabata, S. & Sakurai, H. HSF1 transcriptional activity is modulated by IER5 and PP2A/B55. *FEBS Letters* **589**, 1150–1155 (2015).
22. Kawabata, S., Ishita, Y., Ishikawa, Y. & Sakurai, H. Immediate-early response 5 (IER5) interacts with protein phosphatase 2A and regulates the phosphorylation of

ribosomal protein S6 kinase and heat shock factor 1. *FEBS Letters* **589**, 3679–3685 (2015).

23. Jumper, J. *et al.* Highly accurate protein structure prediction with AlphaFold. *Nature 2021 596:7873* **596**, 583–589 (2021).
24. Kumar, M. *et al.* ELM—the eukaryotic linear motif resource in 2020. *Nucleic Acids Research* **48**, D296–D306 (2020).
25. Fowle, H. *et al.* Pp2a/b55a substrate recruitment as defined by the retinoblastoma-related protein p107. *eLife* **10**, 1–26 (2021).
26. Cundell, M. J. *et al.* A PP2A-B55 recognition signal controls substrate dephosphorylation kinetics during mitotic exit. *The Journal of Cell Biology* **214**, 539 (2016).
27. Yamano, S., Kimura, M., Chen, Y., Imamoto, N. & Ohki, R. Nuclear import of IER5 is mediated by a classical bipartite nuclear localization signal and is required for HSF1 full activation. *Experimental Cell Research* **386**, 111686 (2020).
28. van Kempen, M. *et al.* Fast and accurate protein structure search with Foldseek. *Nature Biotechnology* (2023). doi:10.1038/s41587-023-01773-0
29. Zang, Z. J. *et al.* Identification of PP2A as a novel interactor and regulator of TRIP-Br1. *Cellular Signalling* **21**, 34–42 (2009).
30. Yadav, L. *et al.* Systematic Analysis of Human Protein Phosphatase Interactions and Dynamics. *Cell Systems* **4**, 430-444.e5 (2017).
31. Mirdita, M., Ovchinnikov, S. & Steinegger, M. ColabFold - Making protein folding accessible to all. doi:10.1101/2021.08.15.456425
32. Evans, R. *et al.* Protein complex prediction with AlphaFold-Multimer. *bioRxiv* 2021.10.04.463034 (2022). doi:10.1101/2021.10.04.463034
33. Hsu, S. I. H. *et al.* TRIP-Br: A novel family of PHD zinc finger- and bromodomain-interacting proteins that regulate the transcriptional activity of E2F-1/DP-1. *EMBO Journal* **20**, 2273–2285 (2001).
34. Cho, J. M. *et al.* RBT1, a novel transcriptional co-activator, binds the second subunit of Replication Protein A. *Nucleic Acids Research* **28**, 3478–3485 (2000).
35. Hayashi, R., Goto, Y., Ikeda, R., Yokoyama, K. K. & Yoshida, K. CDCA4 is an E2F transcription factor family-induced nuclear factor that regulates E2F-dependent transcriptional activation and cell proliferation. *Journal of Biological Chemistry* **281**, 35633–35648 (2006).
36. Alerasool, N., Leng, H., Lin, Z.-Y., Gingras, A.-C. & Taipale, M. Identification and functional characterization of transcriptional activators in human cells. *Molecular Cell* **82**, 677-695.e7 (2022).
37. Letourneux, C., Rocher, G. & Porteu, F. B56-containing PP2A dephosphorylate ERK and their activity is controlled by the early gene IEX-1 and ERK. *The EMBO journal* **25**, 727–738 (2006).
38. Rocher, G., Letourneux, C., Lenormand, P. & Porteu, F. Inhibition of B56-containing protein phosphatase 2As by the early response gene IEX-1 leads to control of Akt activity. *Journal of Biological Chemistry* **282**, 5468–5477 (2007).
39. Clark, A. R. & Ohlmeyer, M. Protein phosphatase 2A as a therapeutic target in inflammation and neurodegeneration. *Pharmacology & Therapeutics* **201**, 181 (2019).
40. Ronk, H., Rosenblum, J. S., Kung, T. & Zhuang, Z. Targeting PP2A for cancer therapeutic modulation. *Cancer Biology & Medicine* **19**, 1428 (2022).
41. Fischer, E. S. *et al.* Structure of the DDB1-CRBN E3 ubiquitin ligase in complex with thalidomide. *Nature* **512**, 49 (2014).
42. Punjani, A., Rubinstein, J. L., Fleet, D. J. & Brubaker, M. A. cryoSPARC: algorithms for rapid unsupervised cryo-EM structure determination. *Nature Methods 2017 14:3* **14**, 290–296 (2017).
43. Scheres, S. H. W. RELION: Implementation of a Bayesian approach to cryo-EM structure determination. *Journal of Structural Biology* **180**, 519–530 (2012).
44. Zhu, J. *et al.* A minority of final stacks yields superior amplitude in single-particle cryo-EM. *Nature Communications 2023 14:1* **14**, 1–11 (2023).

45. Scheres, S. H. W. Processing of Structurally Heterogeneous Cryo-EM Data in RELION. *Methods in Enzymology* **579**, 125–157 (2016).
46. Sanchez-Garcia, R. *et al.* DeepEMhancer: a deep learning solution for cryo-EM volume post-processing. *Communications Biology 2021 4:1* **4**, 1–8 (2021).
47. Pettersen, E. F. *et al.* UCSF ChimeraX: Structure visualization for researchers, educators, and developers. *Protein Science* **30**, 70–82 (2021).
48. Croll, T. I. ISOLDE: A physically realistic environment for model building into low-resolution electron-density maps. *Acta Crystallographica Section D: Structural Biology* **74**, 519–530 (2018).
49. Yamashita, K., Palmer, C. M., Burnley, T. & Murshudov, G. N. Cryo-EM single-particle structure refinement and map calculation using Servalcat. *Acta Crystallographica Section D: Structural Biology* **77**, 1282–1291 (2021).
50. Afonine, P. V. *et al.* Real-space refinement in PHENIX for cryo-EM and crystallography. *Acta Crystallographica Section D: Structural Biology* **74**, 531–544 (2018).
51. Nicholls, R. A., Long, F. & Murshudov, G. N. Low-resolution refinement tools in REFMAC5. *Acta Crystallographica Section D: Biological Crystallography* **68**, 404 (2012).
52. Williams, C. J. *et al.* MolProbity: More and better reference data for improved all-atom structure validation. *Protein science : a publication of the Protein Society* **27**, 293–315 (2018).
53. Morin, A. *et al.* Collaboration gets the most out of software. *eLife* **2**, e01456 (2013).
54. Purdie, K. J., Pourreyron, C. & South, A. P. Isolation and Culture of Squamous Cell Carcinoma Lines. *Methods in Molecular Biology* **731**, 151–159 (2011).
55. Liebschner, D. *et al.* Macromolecular structure determination using X-rays, neutrons and electrons: recent developments in Phenix. *urn:issn:2059-7983* **75**, 861–877 (2019).
56. Schmid, E. W. & Walter, J. C. Predictomes: A classifier-curated database of AlphaFold-modeled protein-protein interactions. *bioRxiv* 2024.04.09.588596 (2024). doi:10.1101/2024.04.09.588596
57. Bryant, P., Pozzati, G. & Elofsson, A. Improved prediction of protein-protein interactions using AlphaFold2. *Nature Communications 2022 13:1* **13**, 1–11 (2022).

655 **Figure Legends**

656 **Fig. 1. Cryo-EM structure of a PP2A-IER5 complex and interface analysis.** A, cryo-EM
657 map of the PP2A/B55α-IER5 complex. The scaffolding A subunit is green, the regulatory B55α
658 subunit is purple, the catalytic C subunit is wheat, and IER5 is cyan. B**,** cartoon rendering of
659 the modelled structure, with iron and zinc atoms of the catalytic subunit rendered as brown
660 and grey spheres, respectively. C, Open book view depicting the interface between B55α and
661 IER5 using a surface representation. IER5 is cyan, and B55α is purple, with residues at the
662 contact interface between B55α and IER5 colored pink and dark blue, respectively. D,
663 Electrostatic surface representation of the complex (center), of B55α alone (left), and IER5
664 alone (right), colored on a sliding scale from blue to red (blue: basic, red: acidic). The catalytic
665 and scaffolding subunits have been removed for clarity in panels C and D. See also
666 Supplementary Figs. 1-4 and Table S1.

667

668 **Fig. 2. Intermolecular contacts between B55α and IER5.** A, Overview of the IER5 interface
669 with B55α. The B55α regulatory subunit is rendered as a purple cartoon with a transparent
670 surface and IER5-N50 is cyan, with structural elements of the IER5 helix-loop-helix identified
671 with black labels. B and C, Close-up views highlighting intermolecular contacts between B55α
672 and IER5. Side chains of interacting residues are shown as sticks in CPK colors, with IER5
673 carbon atoms in green and B55α carbon atoms in yellow. Hydrogen bonds are depicted using
674 dashed red lines. B, Interactions of helices 1 and 2 with B55α. The left side shows IER5 helix
675 1 in the foreground and the right side shows IER5 helix 2 in the foreground after a 180° rotation.
676 C, Interactions between the loop of IER5 and B55α. D, Western blot analysis of
677 immunoprecipitates prepared with anti-HA from I5 cells expressing wild-type or mutant HA-
678 tagged IER5 and endogenous B55α. See also Supplementary Fig. 4.

679

680 **Fig. 3. Tau dephosphorylation assay.** A and B, anti-pTau (S396) Western blots comparing
681 the pTau phosphatase activity of PP2A in the presence of increasing concentrations (slanted
682 triangle) of added inhibitory protein. A, Effect of IER5-N50, IER5-N50-K17E, and FAM122A on
683 Tau dephosphorylation. B, effect of IER5-FL and IER5-FL-K17E on Tau dephosphorylation. C,
684 Plot of phosphatase activity as a function of inhibitor concentration for the five proteins tested,
685 based on densitometry analysis. Data represent mean ± s.d. of three independent replicates.
686 Data are normalized to the control condition without PP2A/B55α or inhibitor proteins. Data
687 points were fitted using a log(inhibitor) vs. response (variable slope, four parameters) least
688 squares fit model in Prism. The curves were used to estimate the IC50 value for each protein.
689 See also Supplementary Fig. 5.

690

691 **Fig. 4. Effects of IER5 mutations and deletions on downstream signaling responses.** A,
692 Experimental design for controlled activation of Notch1 by GSI washout. The readout for IER5
693 dependence in keratinocyte differentiation is the induction of *KRT1* expression (figure design
694 adapted from ref. [19]). B, RT-qPCR analysis of *KRT1* RNA abundance measured 72 h after GSI
695 washout in I5 cells expressing wild-type or mutant forms of IER5-FL. Data points are from
696 biological replicates (n = 6). C, F, I, Schematic representations of IER5 constructs analyzed in
697 panels D-E, G-H, and J-K, respectively. D, G, J, RT-qPCR analysis of *KRT1* RNA abundance
698 measured 72 h after GSI washout in I5 cells expressing the indicated protein constructs. Data
699 points are from biological replicates (n=3). E, H, K, Western blots showing the amount of
700 expressed protein for the variants tested in panels D, G, and J, respectively. For each data
701 set, transcript abundance was normalized against GAPDH, and error bars represent standard
702 deviations of the mean. Student's two-tailed T-test (*$P < 0.05$, **$P < 0.01$, ***$P < 0.001$, and
703 ****$P < 0.0001$) was used to compare the means between IER5-FL and IER5-FL test
704 constructs.

705

706 **Fig. 5. Identification of sequence and structural homology between IER family members**
707 **and SERTA domain containing proteins.** A, Searching the human alphafold predicted
708 proteome using IER5 as input in Foldseek[28] led to the identification of CDCA4 and SRTD2 as
709 structural homologues. B, Multiple sequence alignment focusing on the helix-loop-helix motif
710 of IER5, aligning IER, SRTAD, and CDCA4 proteins. The helix 1 and helix 2 segments of IER5
711 seen in the structure of the PP2A/B55α complex with IER5-N50 are indicated above the
712 alignment. Red dots indicate sites of mutations in IER5 that interfere with co-
713 immunoprecipitation of B55α. The alignment is shown using the Zappo color scheme for the
714 20 amino acids: pink, aliphatic; green, hydrophilic; blue, basic; red, acidic; orange, aromatic;
715 yellow, cysteine; magenta, proline or glycine. C, Helical wheel diagram of IER5 helix 1 and
716 helix 2 (left) and a consensus for helix 1 and 2 based on residue conservation among aligned
717 IER, SRTAD and CDCA4 proteins (aliphatic and aromatic residues are denoted as F or W,
718 respectively). The helical face directed at B55α is marked by a magenta arc. D, Best scoring
719 structural models for alphafold2-predicted interactions of IER, SERTAD and CDCA4 proteins
720 with PP2A/B55α. IER, SERTAD, and CDCA4 predictions were restricted to the aligned region
721 in (B). B55α is magenta, the PP2A catalytic subunit is wheat, the PP2A scaffolding subunit is
722 green, and the predicted interactor is cyan. See also Table S1.

723

724 **Supplementary Fig. 1, related to Fig. 1. Alphafold2 prediction of IER5 structure and**
725 **PP2A/B55α-IER5 purification for cryo-EM structure determination.** A and B, Alphafold2[31]
726 prediction of the IER5 structure, shown in cartoon representation. A, pLDDT coloring of IER5
727 using alphafold palette: <50, red, very low confidence; 50-70, yellow, low confidence; 70-90,
728 light blue, confident; 90-100, dark blue, very high confidence. B, Cartoon representation of
729 IER5 with the IER-N50 domain colored cyan. The 1-50 region is also highlighted in cyan on
730 the domain representation beneath the cartoon. C, Size exclusion chromatogram of the
731 purified PP2A/B55α-IER5 complex on a Superdex 200 column. An SDS-PAGE gel of the

732 purified complex is shown to the right of the chromatogram. Both peaks are PP2A/B55α-IER5
733 complexes; peak 2 was used in all biochemical and structural studies.

734

735 **Supplementary Fig. 2, related to Fig. 1. Cryo-EM image processing workflow.** Cryo-EM
736 processing scheme for PP2A/B55α-IER5 reconstruction. Milestone maps are shown to display
737 progression of processing (the discarded, "junk" class is shown as pink, the monomer as
738 orange, the dimer as blue, and the combined map as purple). The masks used for local
739 refinement are light blue.

740

741 **Supplementary Fig. 3, related to Fig. 1. Cryo-EM data quality.** A, Representative
742 micrograph of PP2A-IER5 in vitreous ice visualized by cryo-EM on a Titan Krios microscope
743 equipped with a Gatan K3 detector. Scale bar indicates 500 Å. B, GS-FSC curves with default
744 CryoSPARC masks. C, Orientation distribution of particles (from CryoSPARC) used in
745 preparing the final map of PP2A/B55α-IER5 for model building. D, 2D class averages of
746 PP2A/B55α-IER5 reconstruction prior to particle subtraction. E, Local resolution map of the
747 final map generated by CryoSPARC (FSC threshold = 0.143). F, map-model FSC curve (line
748 at FSC = 0.5) generated using Phenix[55]. G, Maps around IER5 helix 1 (left), loop (loop) and
749 helix 2 (right). Sigma was set to 3. All maps shown were processed using DeepEMhancer[46].

750

751 **Supplementary Fig. 4, related to Figs. 1 and 2. Comparison of the PP2A/B55α - IER5**
752 **complex with PP2A/B55α structures bound to other partners.** A, superposition of
753 PP2A/B55α bound to microcystin-LR[9] (MC-L complex, protein subunits in gray, microcystin-
754 LR as salmon sticks) on the structure of the PP2A/B55α complex with IER5. In the IER5
755 complex, the B55α subunit is purple, the catalytic subunit is wheat, the scaffolding subunit is
756 green, and IER5 is cyan. Helices are depicted as solid cylinders. Alignment was performed on
757 the B55α subunit. Note the increased curvature of the scaffolding subunit and the 22 Å

758 displacement of its C terminus in the IER5 structure relative to the microcystin-LR structure.
759 B, Comparison showing the different binding modes of IER5, ARPP19 and FAM122A when
760 bound to PP2A/B55α[11]. Structures are shown in cartoon representation with a transparent
761 surface. The three PP2A subunits are colored as in (A), with IER5 in cyan, ARPP19 in blue,
762 and FAM122A in red. Structures were aligned on the B55α subunit. C, Surface representations
763 of B55α (purple) with bound IER5-N50 (cyan) shown in cartoon representation. On each copy,
764 surface residues of B55α important for IER5-N50 binding or substrate recruitment are painted
765 a different color from left to right: IER5-N50, pink surface; p107[25], blue surface; PRC1[26], yellow
766 surface; pTau[9], green surface.

767

768 **Supplementary Fig. 5, related to Figs. 1 and 2.** A, Size exclusion chromatogram of the
769 purified PP2A/B55α complex on a Superdex 200 column. An SDS-PAGE gel of the purified
770 complex is shown to the right of the chromatogram. The peak at approximately 20 mL elution
771 volume corresponds to the FLAG peptide. B, SDS-PAGE gels of purified MBP-fusions for
772 IER5-N50, IER5-N50 K17E, IER5-FL and IER5-FL K17E.

773 **Table 1. Cryo-EM data collection, refinement and validation statistics.**

PP2A/B55α-IER5 EMD-42428 ([https://www.ebi.ac.uk/emdb/EMD42428). PDB 8UO5 ([http://doi.orgXXX/])	
Data collection and processing	
Voltage (kV)	300
Electron exposure ($e^-/Å^{-2}$)	53.7
Defocus range (μm)	0.8 – 2.0
Pixel size (Å)	0.825
Symmetry imposed	C1
Initial particle images (no.)	3,950,110
Final particle images (no.)	66,568
FSC threshold	0.143
Refinement	
Initial model used	Alphafold (AF-Q5VY09-F1) PP2A/B55α-FAM122A (PDB:8so0)
Map Resolution (Å)	3.27
Map resolution range (Å) (per atom position)	2.06 – 5.38
Model composition	
Non-hydrogen atoms	10,218
Protein residues	1,303
Ligands	Fe: 1, Zn:1
B factors ($Å^2$)	
Protein	164
Ligand	170
R.M.S.D. deviations	
Bond lengths (Å)	0.011
Bond angles (°)	1.455
Validation	
MolProbity score	1.47
Clashscore	4.28
Poor rotamers (%)	0.81
CaBLAM outliers (%)	0.95
CCmask	0.76
CCvolume	0.76
Map-to-model FSC (FSC = 0.5)	3.66
Ramachandran plot	
Favoured (%)	96.18
Allowed (%)	3.82
Disallowed (%)	0.00

774

775

776 **Table S1, related to Fig. 5. Predictions of complex structures between IER/SERTAD**

777 **superfamily proteins and PP2A/B55α.** Structures of complexes between IER, SERTAD, and

CDCA4 proteins with PP2A/B55α heterotrimers were predicted using alphafold2[31] (Fig. 5) and scored using predictomes[56]. Each column shows a metric used to score the predictive value of the model. Average models indicate the mean number of interface contacts observed for the five models that were generated. The maximum (max) number of models counts how many models share one or more of the predicted contacts in other models. Predicted Dockq (pDOCKq) is a metric that incorporates the alphafold2 pLDDT scores across the predicted protein-protein interaction interface[57]. Predicted local distance difference test (pLDDT), and predicted alignment error (PAE) are alphafold2 metrics[31].

Protein	average models	max number of models	best model	best model pDockQ	best model pLDDT	best model PAE
SRTD4	4.8	5	4	0.713	87.7	1.8
SRTD2	4.7	5	4	0.72	90	1.6
STD1	4.7	5	4	0.722	91.5	1.4
CDCA4	4.6	5	4	0.715	89.9	1.6
IER5	4.5	5	4	0.714	88.1	1.6
IER5L	4.4	5	4	0.714	88.5	1.4
IER2	4.4	5	4	0.713	87.7	1.7
SRTD3	4.4	5	3	0.714	88.1	1.7

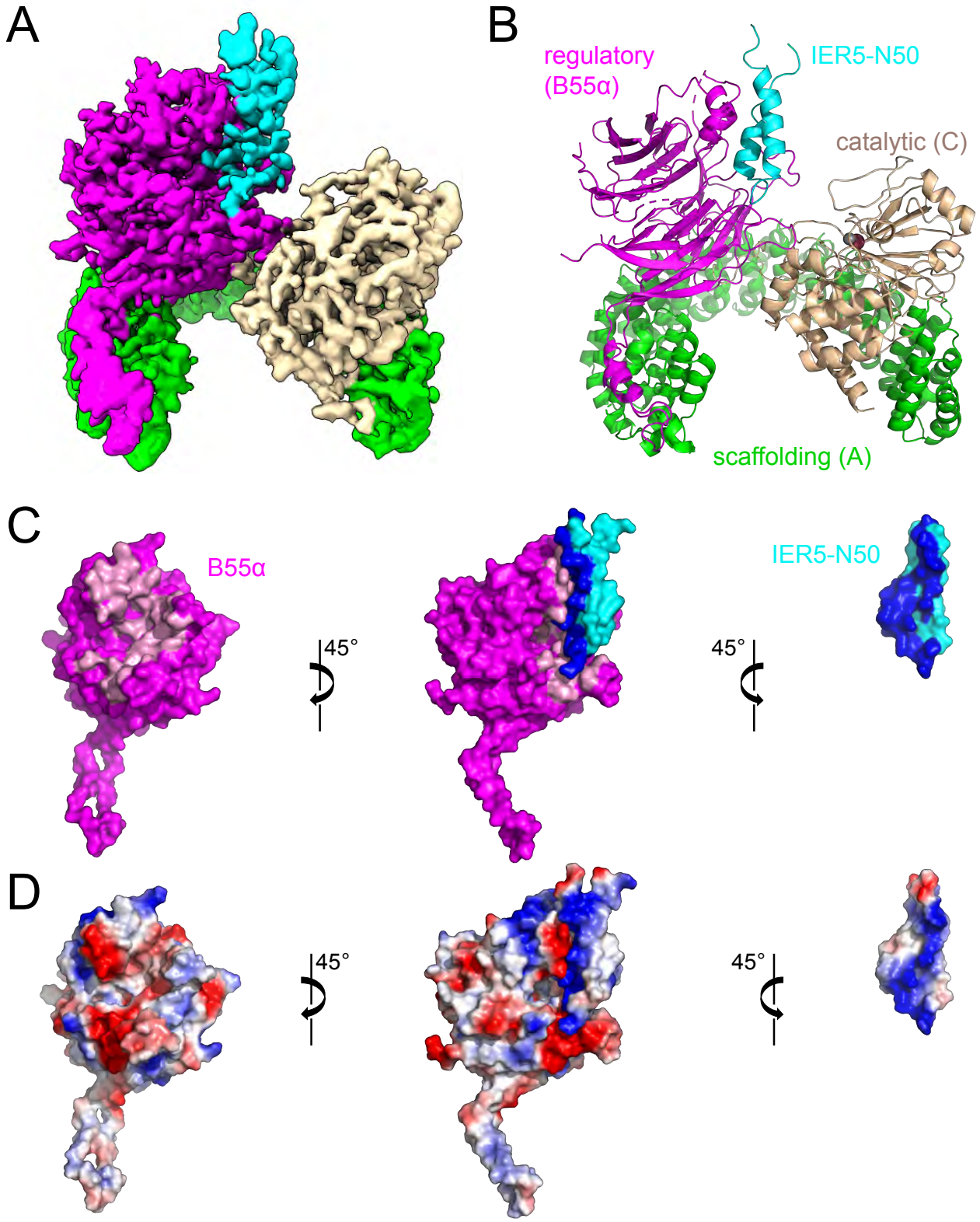
A
B
regulatory
(B55α)
IER5-N50
catalytic (C)
scaffolding (A)
C
B55α
45°
45°
IER5-N50
D
45°
45°

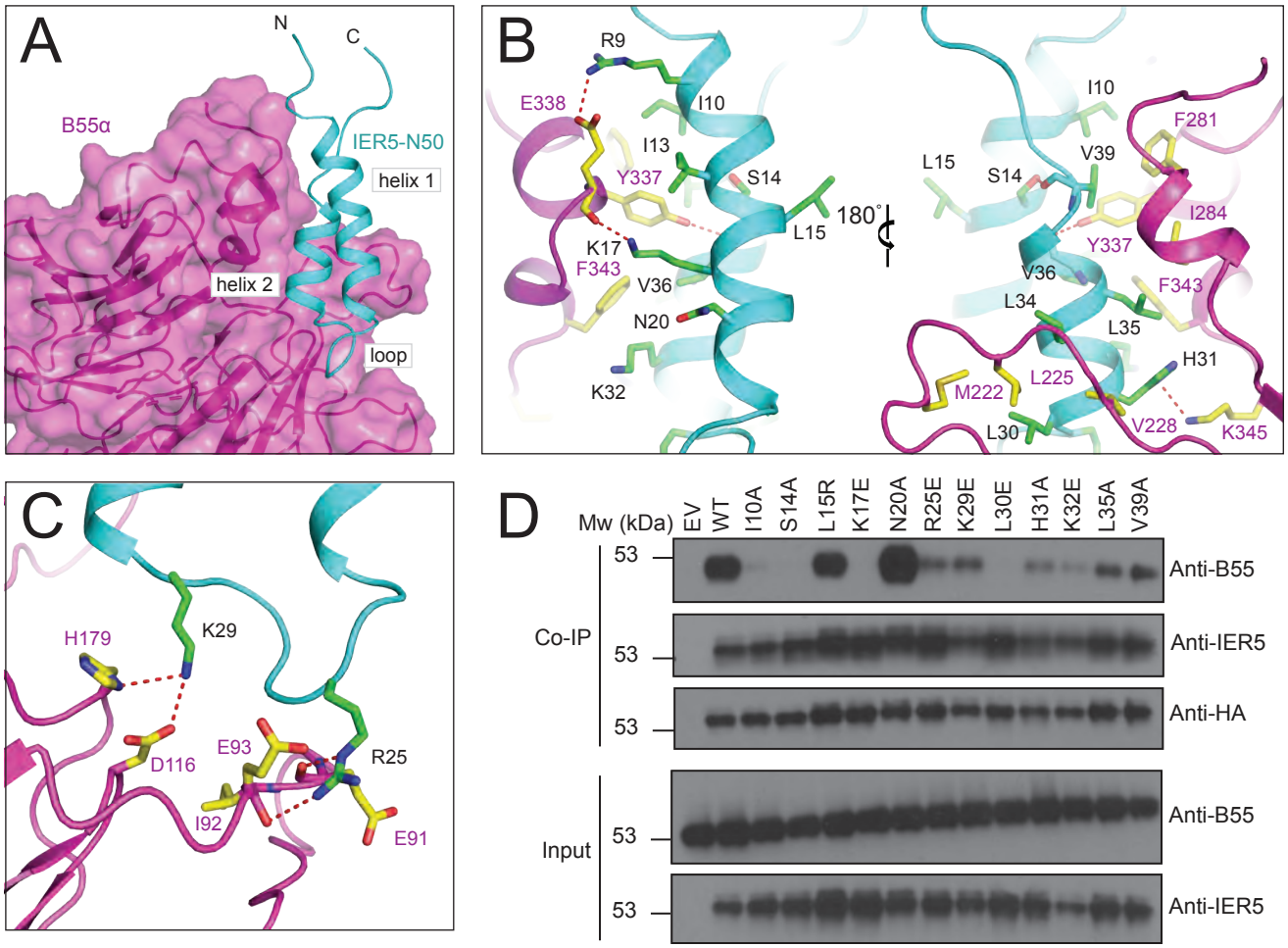
A
N
C
B55α
IER5-N50
helix 1
helix 2
loop
B
R9
E338
I10
I13
Y337
S14
L15
180°
K17
F343
V36
N20
K32
I10
F281
L15
S14
V39
I284
Y337
V36
F343
L34
L35
H31
L225
M222
V228
K345
L30
C
H179
K29
D116
E93
R25
I92
E91
D
Mw (kDa)
EV
WT
I10A
S14A
L15R
K17E
N20A
R25E
K29E
L30E
H31A
K32E
L35A
V39A
Co-IP
Input
53
Anti-B55
Anti-IER5
Anti-HA

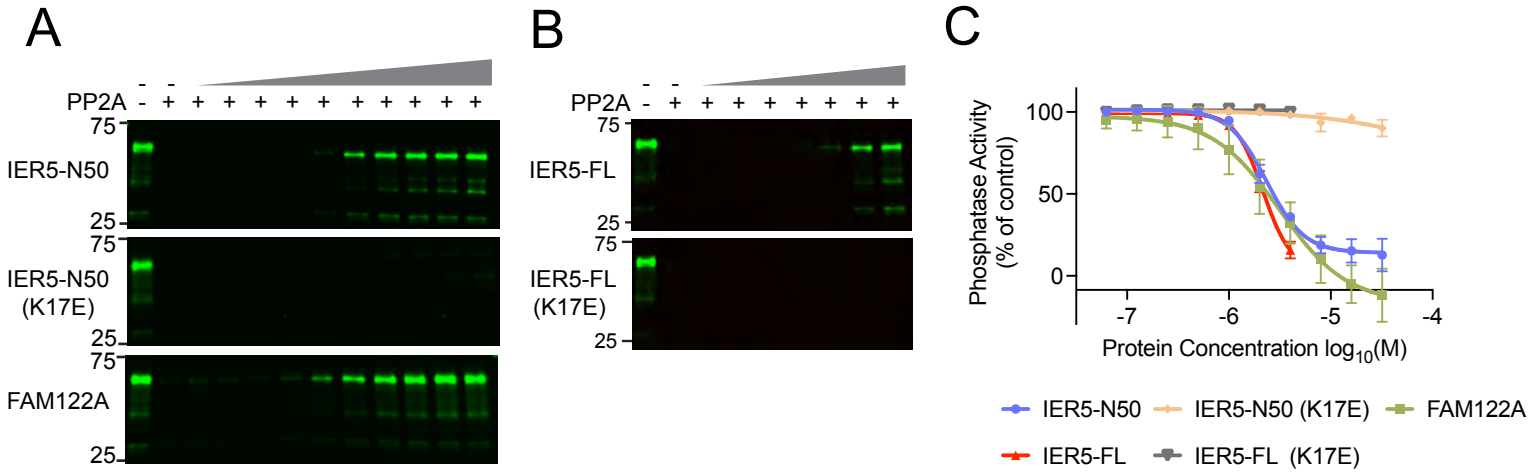
A
PP2A
IER5-N50
IER5-N50 (K17E)
FAM122A
75
25
B
PP2A
IER5-FL
IER5-FL (K17E)
75
25
C
Phosphatase Activity (% of control)
100
50
0
-7
-6
-5
-4
Protein Concentration log10(M)
IER5-N50
IER5-N50 (K17E)
FAM122A
IER5-FL
IER5-FL (K17E)

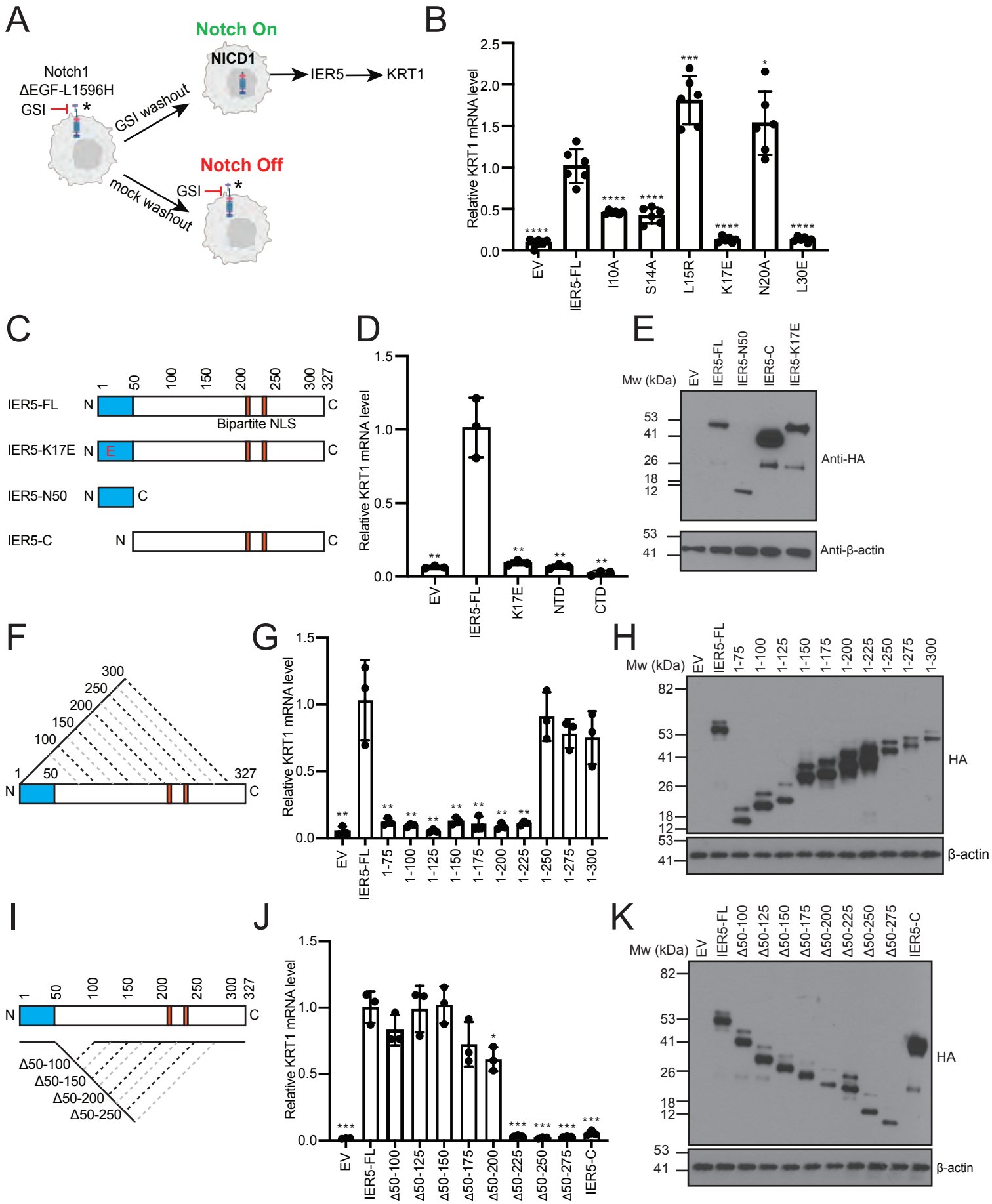
A
Notch On
NICD1
IER5
KRT1
Notch1
ΔEGF-L1596H
GSI
GSI washout
Notch Off
GSI
mock washout
B
Relative KRT1 mRNA level
EV
IER5-FL
I10A
S14A
L15R
K17E
N20A
L30E
C
IER5-FL
IER5-K17E
IER5-N50
IER5-C
Bipartite NLS
D
Relative KRT1 mRNA level
EV
IER5-FL
K17E
NTD
CTD
E
Mw (kDa)
EV
IER5-FL
IER5-N50
IER5-C
IER5-K17E
Anti-HA
Anti-β-actin
F
G
Relative KRT1 mRNA level
EV
IER5-FL
1-75
1-100
1-125
1-150
1-175
1-200
1-225
1-250
1-275
1-300
H
Mw (kDa)
HA
β-actin
I
Δ50-100
Δ50-150
Δ50-200
Δ50-250
J
Relative KRT1 mRNA level
EV
IER5-FL
Δ50-100
Δ50-125
Δ50-150
Δ50-175
Δ50-200
Δ50-225
Δ50-250
Δ50-275
IER5-C
K
Mw (kDa)
HA
β-actin

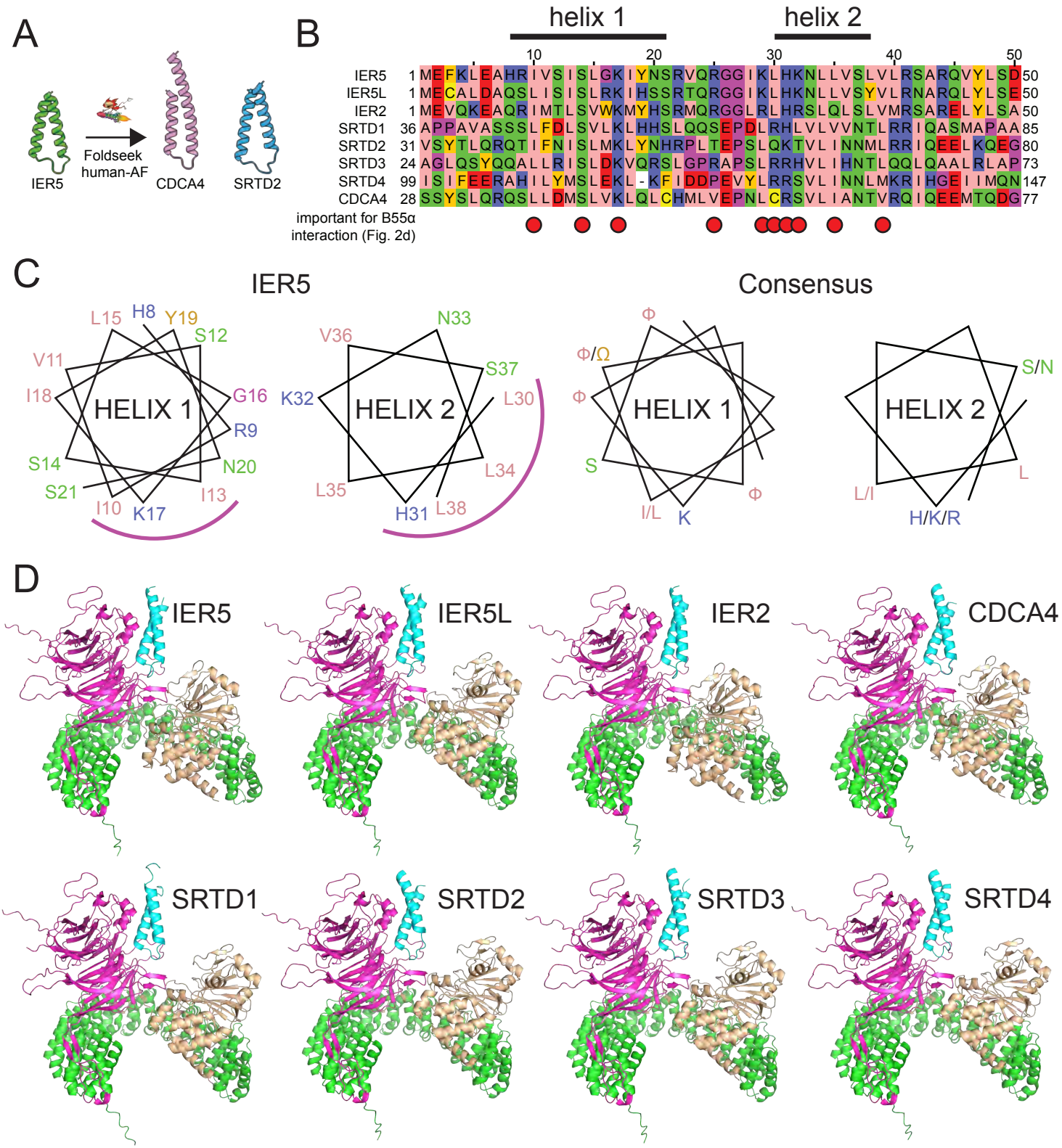
A
IER5
Foldseek
human-AF
CDCA4
SRTD2
B
helix 1
helix 2
10
20
30
40
50
IER5 1 MEFKLEAHRIVSISLGKIYNSRVQRGGIKLHKNLLVSLVLRSARQVYLSD 50
IER5L 1 MECALDAQSLISISLRKIHSSRTQRGGIKLHKNLLVSYVLRNARQLYLSE 50
IER2 1 MEVQKEAQRIMTLSVWKMYHSRMQRGGLRLHRSLQLSLVMRSARELYLSA 50
SRTD1 36 APPAVASSSLFDLSVLKLHHSLQQSEPDLRHLVLVVNTLRRIQASMAPAA 85
SRTD2 31 VSYTLQRQTIFNISLMKLYNHRPLTEPSLQKTVLINNMLRRIQEELKQEG 80
SRTD3 24 AGLQSYQQALLRISLDKVQRSLGPRAPSLRRHVLIHNTLQQLQAALRLAP 73
SRTD4 99 ISIFEERAHILYMSLEKL-KFIDDPEVYLRRSVLINNLMKRIHGEIIMQN 147
CDCA4 28 SSYSLQRQSLLDMSLVKLQLCHMLVEPNLCRSVLIANTVRQIQEEMTQDG 77
important for B55α
interaction (Fig. 2d)
C
IER5
Consensus
L15
H8
Y19
S12
V11
I18
G16
R9
S14
N20
S21
I13
I10
K17
HELIX 1
V36
N33
S37
K32
L30
L34
L35
H31
L38
HELIX 2
Φ
Φ/Ω
Φ
S
Φ
I/L
K
HELIX 1
S/N
L
L/I
H/K/R
HELIX 2
D
IER5
IER5L
IER2
CDCA4
SRTD1
SRTD2
SRTD3
SRTD4

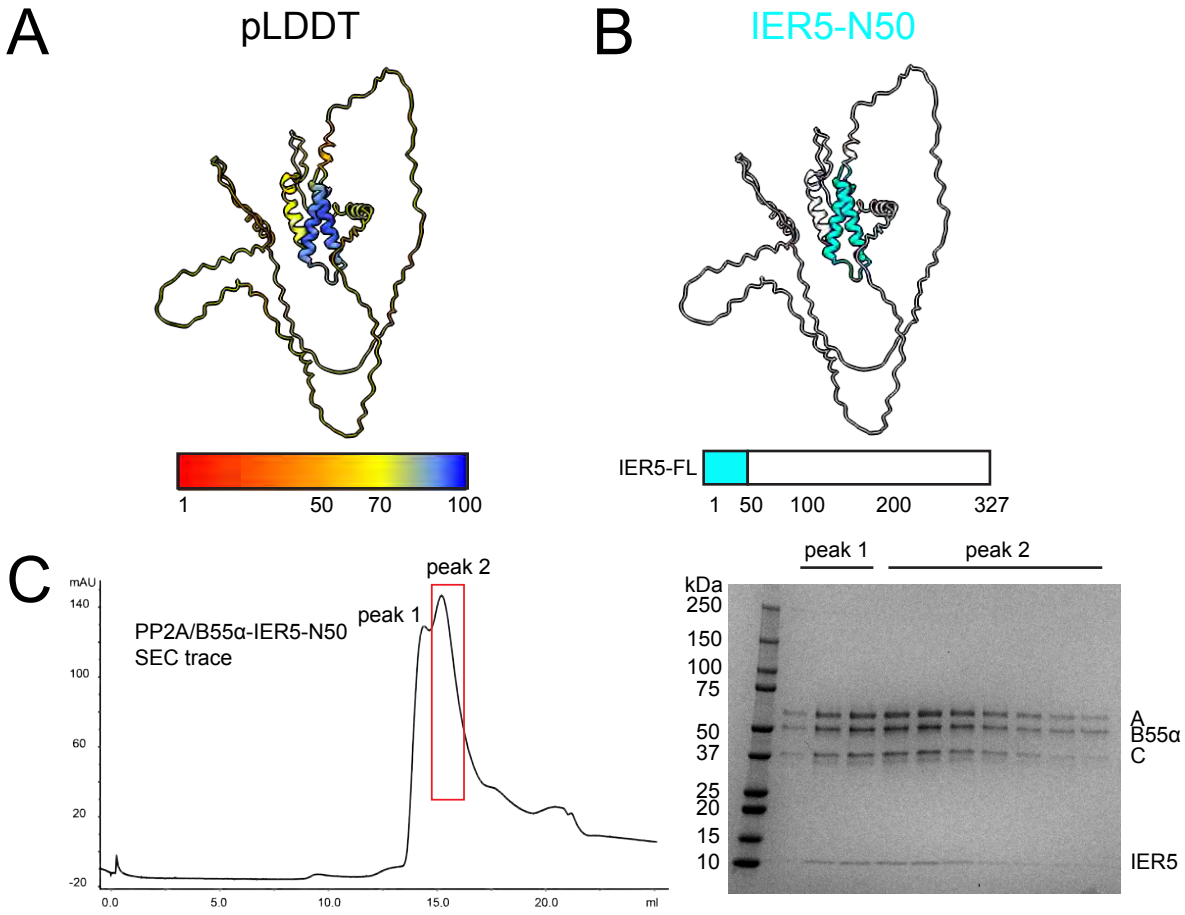
A
pLDDT
1
50
70
100
B
IER5-N50
IER5-FL
1
50
100
200
327
C
PP2A/B55α-IER5-N50
SEC trace
peak 1
peak 2
mAU
140
100
60
20
-20
0.0
5.0
10.0
15.0
20.0
ml
peak 1
peak 2
kDa
250
150
100
75
50
37
25
20
15
10
A
B55α
C
IER5

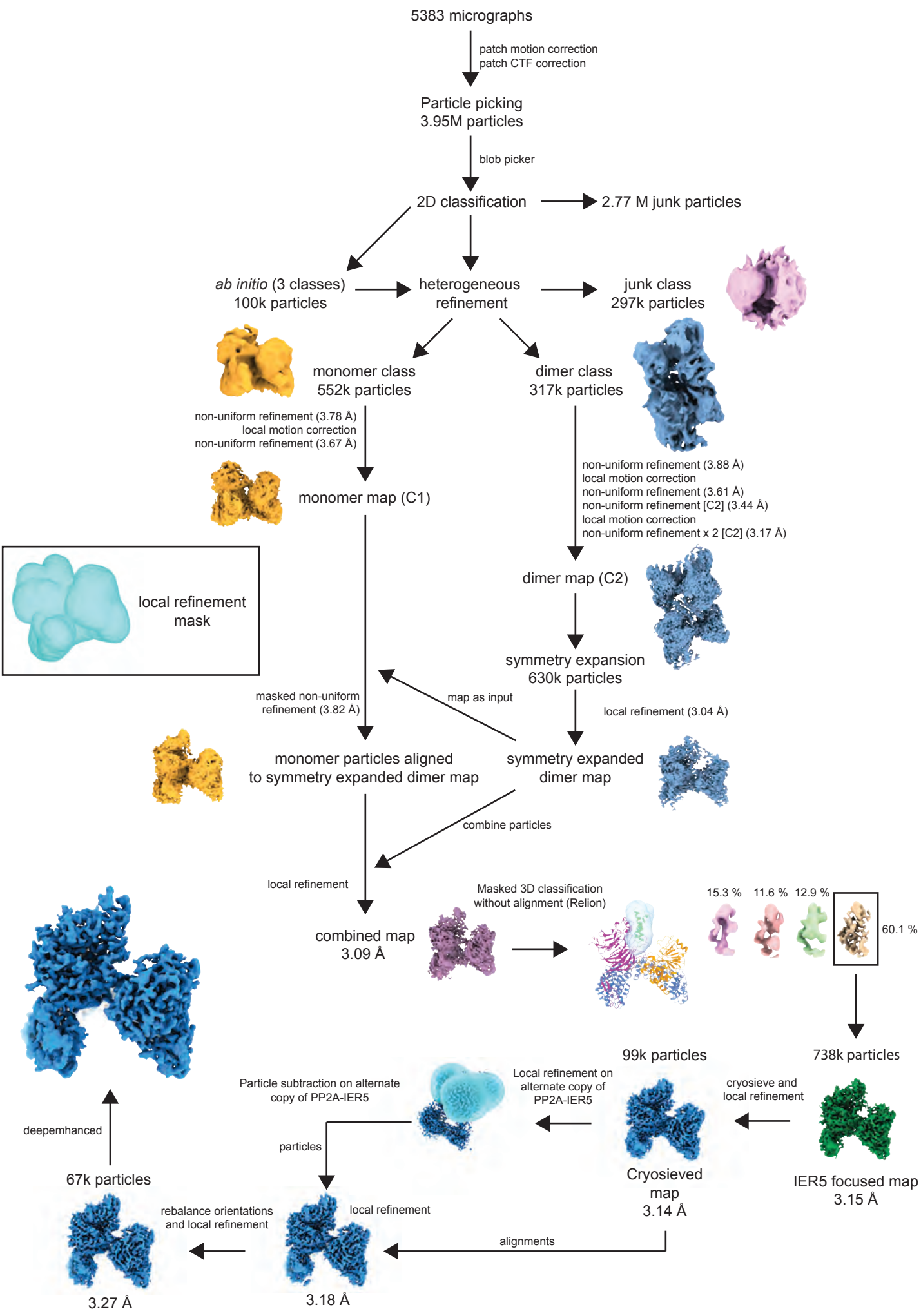
5383 micrographs
patch motion correction
patch CTF correction
Particle picking
3.95M particles
blob picker
2D classification
2.77 M junk particles
ab initio (3 classes)
100k particles
heterogeneous refinement
junk class
297k particles
monomer class
552k particles
dimer class
317k particles
non-uniform refinement (3.78 Å)
local motion correction
non-uniform refinement (3.67 Å)
monomer map (C1)
non-uniform refinement (3.88 Å)
local motion correction
non-uniform refinement (3.61 Å)
non-uniform refinement [C2] (3.44 Å)
local motion correction
non-uniform refinement x 2 [C2] (3.17 Å)
dimer map (C2)
local refinement mask
symmetry expansion
630k particles
masked non-uniform refinement (3.82 Å)
map as input
local refinement (3.04 Å)
monomer particles aligned to symmetry expanded dimer map
symmetry expanded dimer map
combine particles
local refinement
combined map
3.09 Å
Masked 3D classification without alignment (Relion)
15.3 %
11.6 %
12.9 %
60.1 %
99k particles
738k particles
Particle subtraction on alternate copy of PP2A-IER5
Local refinement on alternate copy of PP2A-IER5
cryosieve and local refinement
deepemhanced
particles
67k particles
Cryosieved map
3.14 Å
IER5 focused map
3.15 Å
rebalance orientations and local refinement
local refinement
alignments
3.27 Å
3.18 Å

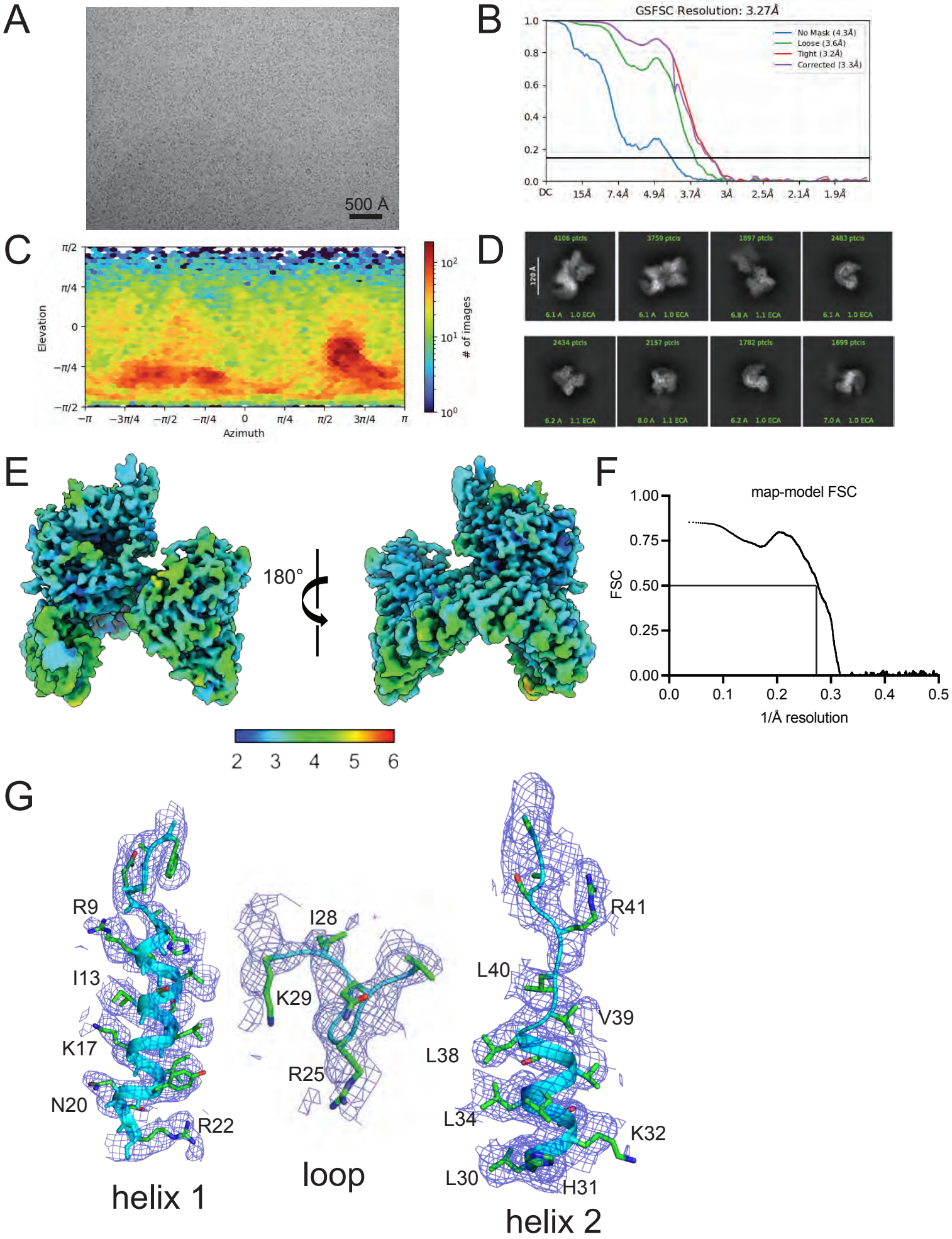
A
500 Å
B
GSFSC Resolution: 3.27Å
No Mask (4.3Å)
Loose (3.6Å)
Tight (3.2Å)
Corrected (3.3Å)
DC
15Å
7.4Å
4.9Å
3.7Å
3Å
2.5Å
2.1Å
1.9Å
C
Elevation
Azimuth
# of images
D
4106 ptcls
3759 ptcls
1897 ptcls
2483 ptcls
2434 ptcls
2157 ptcls
1782 ptcls
1699 ptcls
120 Å
E
180°
2 3 4 5 6
F
map-model FSC
FSC
1/Å resolution
G
R9
I13
K17
N20
R22
helix 1
I28
K29
R25
loop
R41
L40
V39
L38
L34
K32
L30
H31
helix 2

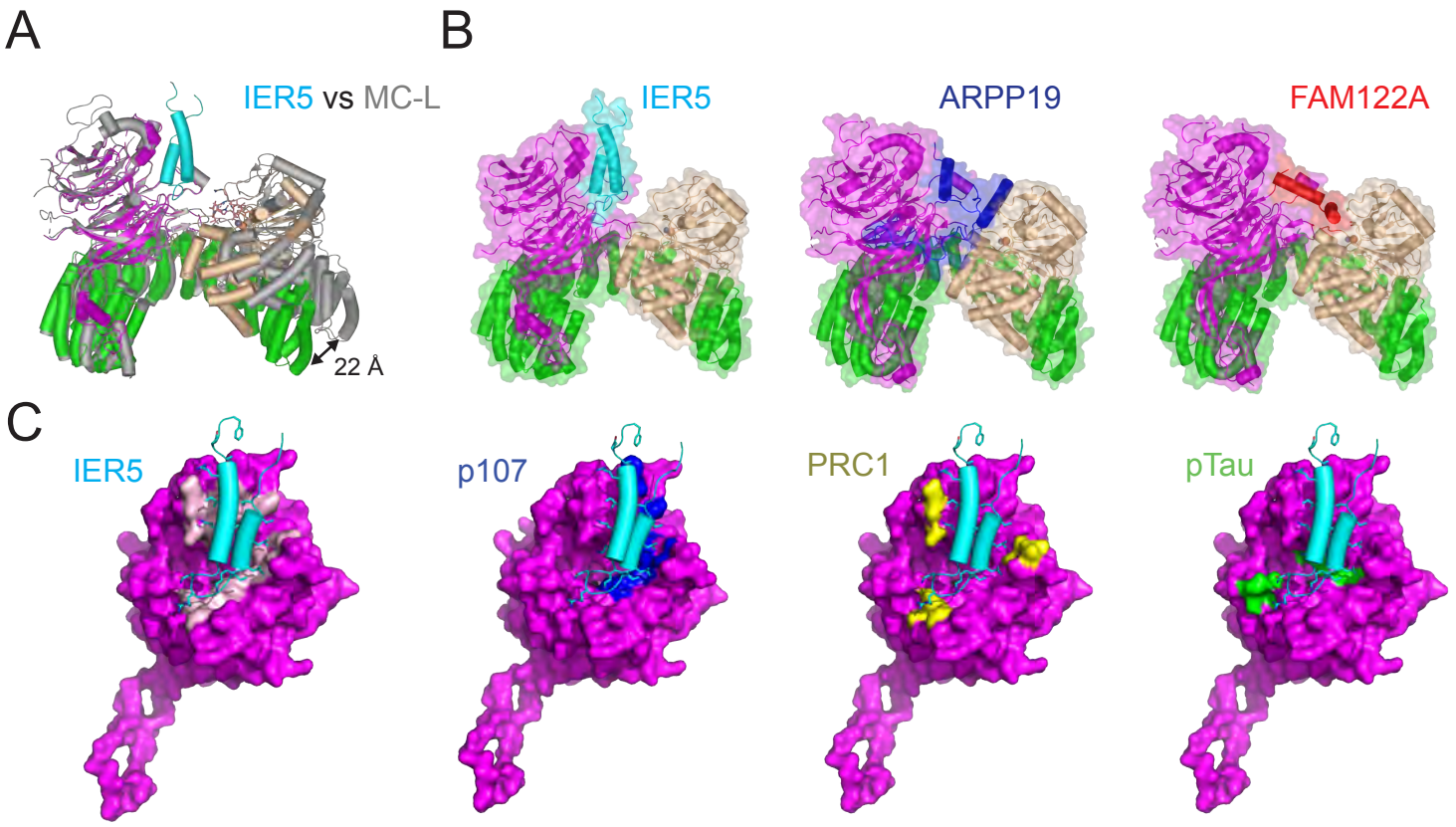
A
IER5 vs MC-L
22 Å
B
IER5
ARPP19
FAM122A
C
IER5
p107
PRC1
pTau

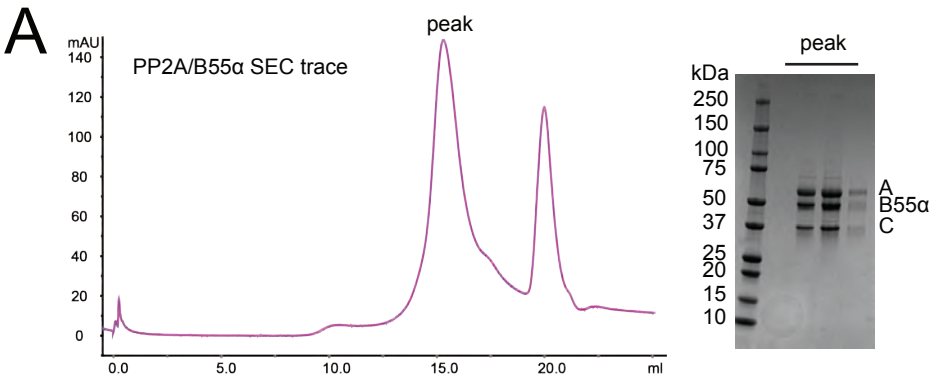
A
PP2A/B55α SEC trace
peak
mAU
140
120
100
80
60
40
20
0
0.0
5.0
10.0
15.0
20.0
ml
peak
kDa
250
150
100
75
50
37
25
20
15
10
A
B55α
C

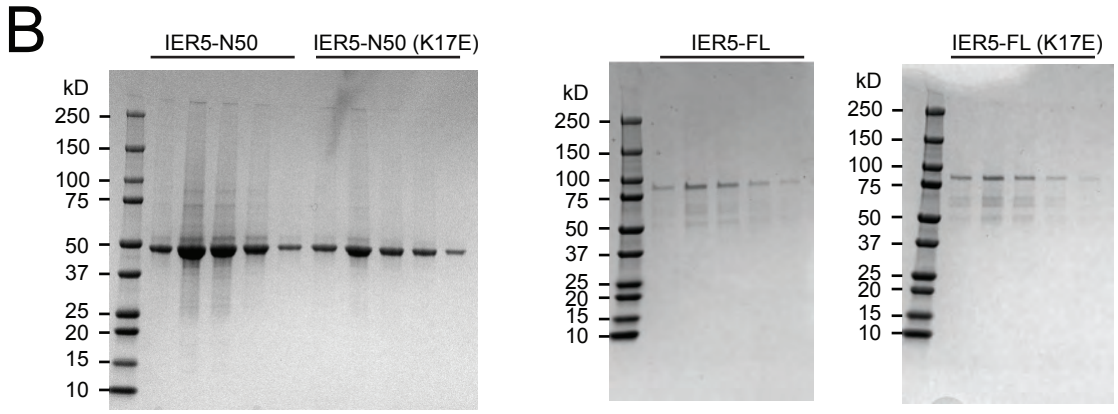
B
IER5-N50
IER5-N50 (K17E)
IER5-FL
IER5-FL (K17E)
kD
250
150
100
75
50
37
25
20
15
10